Photophysics of Point Defects in ZnO Nanoparticles

ARTICLE *in* ADVANCED OPTICAL MATERIALS · FEBRUARY 2015

Impact Factor: 4.06 · DOI: 10.1002/adom.201400592

6 AUTHORS, INCLUDING:

Sumin Choi
University of Technology Sydney
10 PUBLICATIONS **21** CITATIONS
SEE PROFILE

Matthew R Phillips
University of Technology Sydney
221 PUBLICATIONS **2,444** CITATIONS
SEE PROFILE

Bruce Cowie
Australian Synchrotron
102 PUBLICATIONS **1,915** CITATIONS
SEE PROFILE

Cuong Ton-That
University of Technology Sydney
54 PUBLICATIONS **957** CITATIONS
SEE PROFILE

Photophysics of Point Defects in ZnO Nanoparticles

*Sumin Choi, Matthew R. Phillips, Igor Aharonovich, Soraya Pornsuwan, Bruce C. C. Cowie, and Cuong Ton-That**

Zinc oxide (ZnO) nanoparticles have recently been identified as a promising candidate for advanced nanophotonics applications and quantum technologies. This work reports the formation of luminescent point defects and describes their photophysical properties. In particular, it is shown using correlative photoluminescence, cathodoluminescence, electron paramagnetic resonance (EPR), and X-ray absorption near-edge spectroscopy that green luminescence at 2.48 eV and an EPR line at $g = 2.00$ belong to a surface oxygen vacancy ($V_{o,s}^{+}$) center, while a second green emission at 2.28 eV is associated with zinc vacancy (V_{Zn}) centers. It is established that radiative point defects can be excited in the visible that exhibits nanosecond lifetimes using both above bandgap and sub-bandgap 405 and 532 nm excitation. This work provides important knowledge towards employment of point defects in ZnO in nanophotonics technologies.

1. Introduction

Zinc oxide (ZnO) offers attractive optical, mechanical, and electronic properties, including a large exciton binding energy (60 meV), a high dielectric constant, high carrier saturation velocity, piezoelectric behavior, and low lasing density threshold.[1] One of the most fascinating applications of ZnO is its ability to host bright fluorescent defects that exhibit luminescence across the entire visible range, facilitating extensive applications in lighting technologies.[2,3] Unfortunately, many of the luminescent features are not fully understood and cannot be engineered in a controllable way. For instance, while it is widely acknowledged that substitutional Li_{Zn} (a common impurity in hydrothermal growth) introduces a deep ≈60 meV acceptor level and is responsible for yellow luminescence (YL),[4,5] the chemical origin of green luminescence (GL) remains highly controversial. Earlier works attributed the GL to several native defects including oxygen vacancies (V_O),[6] and zinc vacancies (V_{Zn}),[7] interstitials (Zn_i, O_i),[8] and antisite defects (Zn_O, O_{Zn})[9] as well as chemical impurities such as Cu.[10]

The need to characterize point defects in ZnO is further amplified with the recent applications of ZnO nanoparticles as hosts of single emitters for quantum information processing[11–13] and their use in random lasing[14] and other advanced sensing technologies.[15] These applications require precise control over the defect engineering in ZnO nanoparticles. Consequently, correlative characterization of point defects will be valuable to explore the luminescence properties and affiliate them with their chemical and paramagnetic spin features.

In this work we perform comprehensive studies on the formation and photophysical properties of point defects in ZnO nanoparticles. In particular, we employ correlative characterization techniques to assign the optical emission peaks and electron paramagnetic resonance (EPR) lines to specific defects in ZnO nanoparticles. Our results provide new insight into optical luminescence properties of ZnO nanoparticles and promote them as potential candidate for nanophotonic technologies.[16]

2. Results and Discussion

After being annealed in an Ar or Zn vapor environment at 700–900 °C the as-received ZnO nanoparticles (diameter ≈ 20 nm) coalescence[17,18] and display faceted morphologies (**Figure 1**). The nanoparticles increase in average size up to about 120 nm after annealing in inert gas (Ar) or oxygen, and up to 150 nm for annealing in Zn vapor at 900 °C [see Figures S1 and S2, Supporting Information for nanoparticle sizes obtained from scanning electron microscopy (SEM) image and X-ray diffraction (XRD) analysis]. Since the Bohr radius of ZnO is 2.34 nm,[19] the nanoparticles are large enough to avoid quantum size effects but still possess a sufficiently large surface area to allow defect engineering.

To investigate the occurrence of defects in ZnO nanoparticles, EPR spectroscopy was performed. **Figure 2**a shows EPR spectra of the as-received, O_2 annealed, Zn vapor annealed ZnO nanoparticles and a bare Si(100) substrate for comparison. The as-received ZnO nanoparticles exhibit a strong signal at $g = 1.96$, which has been previously assigned to zinc vacancies (V_{Zn}^{-}),[20] oxygen interstitials (O_i^{-}),[20] zinc interstitials (Zn_i^{+})[21] and to electrons in weakly bound or conduction band (CB)

S. Choi, Prof. M. R. Phillips, Prof. I. Aharonovich, Dr. C. Ton-That
School of Physics and Advanced Materials
University of Technology Sydney
P.O. Box 123, Broadway NSW 2007, Australia
E-mail: Cuong.Ton-That@uts.edu.au
Dr. S. Pornsuwan
Department of Chemistry
Mahidol University
Bangkok, Thailand
Dr. B. C. C. Cowie
Australian Synchrotron
800 Blackburn Road, Clayton VIC 3168, Australia

DOI: 10.1002/adom.201400592

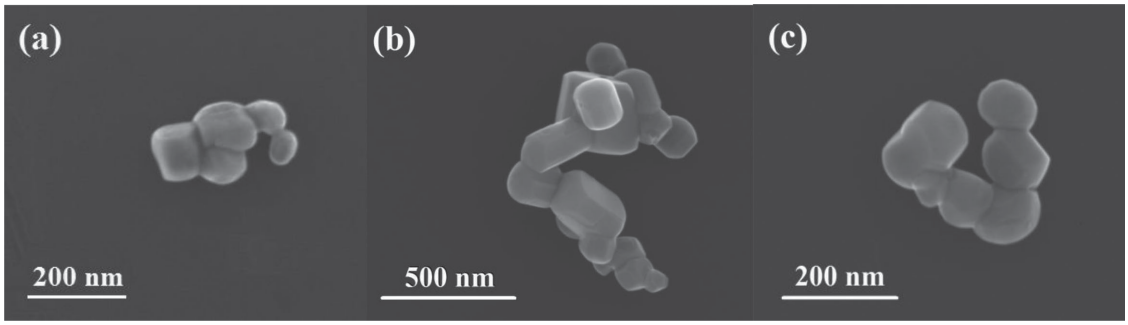

Figure 1. SEM images of the ZnO nanoparticles annealed at a) 700 °C in Zn vapor, b) 900 °C in Zn vapor, and c) 900 °C in Ar. The annealed nanoparticles exhibit highly faceted morphologies and enlargement from the 20 nm as-received size.

states arising from different donor impurities, such as Ga, In, and Al[22,23] and H.[24] A weak signal is also present at $g = 2.00$, which has been attributed to singly ionized oxygen vacancy centers, V_o^+.[25] An EPR signal from a V_o^+ center was unexpected as the reported EPR signal at $g = 2.00$ occurs during photoionization of neutral oxygen vacancies, V_O^0. Computational density functional theory modeling has shown that the V_o center in bulk ZnO behaves as a negative U center and consequently will either spontaneously capture or emit an electron, converting to V_O^0 or V_O^{2+} center respectively.[26] Consequently the presence of the $g = 2.00$ line in the as-received ZnO nanoparticles indicates that its chemical origin is likely related to singly ionized surface oxygen vacancy centers, $V_{O,s}^+$.

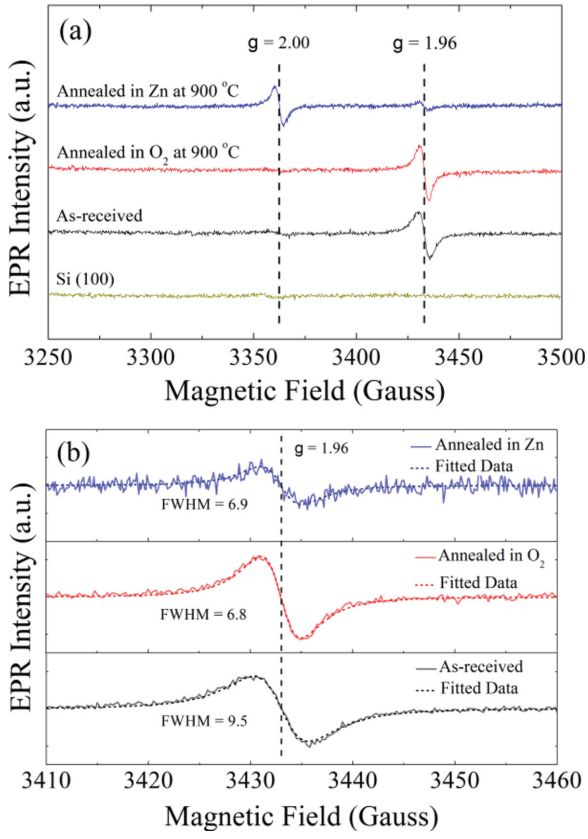

Figure 2. a) EPR spectra of the as-received, O_2 annealed, Zn vapor annealed ZnO nanoparticles, and a bare Si (100) substrate for comparison. Two main types of paramagnetic signals at $g = 2.00$ and 1.96 are observed, corresponding to $V_{O,s}^+$ defects and localized donors, respectively. b) Magnified EPR spectra of the $g = 1.96$ line for the as-received and annealed ZnO nanoparticles, showing a decrease in the EPR linewidth after annealing.

Upon annealing in O_2, the weak signal at $g = 2.00$ vanishes consistent with its assignment to surface $V_{O,s}^+$ defects. Conversely the $g = 1.96$ slightly increases due to an improvement in crystal quality. This result also suggests its assignment to Zn_i or H donors unlikely. Both of these particular defects are highly mobile in ZnO[27,28] and should be annihilated by surface reactions with the O_2 gas during annealing. The thermally induced EPR changes could arise from the stronger presence of V_{Zn} which are created by via chemical surface reactions with gaseous oxygen at elevated temperatures. However, more recent studies have concluded that the EPR signatures for V_{Zn} related centers are located around $g = 2.02$.[29] Accordingly, the $g = 1.96$ line is attributed to the presence of localized donor states as suggested by other workers.[23]

As shown in Figure 2a annealing in Zn vapor produced a strong line at $g = 2.00$ which can be attributed to formation of $V_{O,s}^+$ as described above. This result can be explained by (i) the rapid coalescence of the nanoparticles in an oxygen deficient atmosphere at elevated temperatures,[17] as shown in Figure 1 above, leading to the formation of oxygen vacancies and (ii) surface chemical reactions with Zn vapor that remove oxygen from the surface. In contrast the $g = 1.96$ peak intensity was dramatically reduced after annealing in Zn vapor. This result can be explained by the thermal displacement of donors on Zn sites by Zn_i or via the formation of ionized donor – zinc interstitial defect pairs (D^+–Zn_i^+).[30] A Lorentzian line shape was used to fit the $g = 1.96$ EPR peaks shown in Figure 2a to compare their full width half maximum (FWHM). Figure 2b shows the fitted EPR spectra, which shows the FWHM decreasing from 9.5 to ≈6.8 G after annealing. The narrow EPR lines after annealing indicate an improvement in the crystal quality which increases the average spin–spin distance.[31]

To gain greater insight into the formation of the point defects before and after thermal annealing, X-ray absorption near edge spectroscopy (XANES) measurements were used to probe the local electronic structure of O and Zn atoms in the nanoparticles (**Figure 3**). The Zn L_3-edge spectra before and after annealing in O_2 or Zn vapor environments are shown in

Adv. Optical Mater. 2015,
DOI: 10.1002/adom.201400592

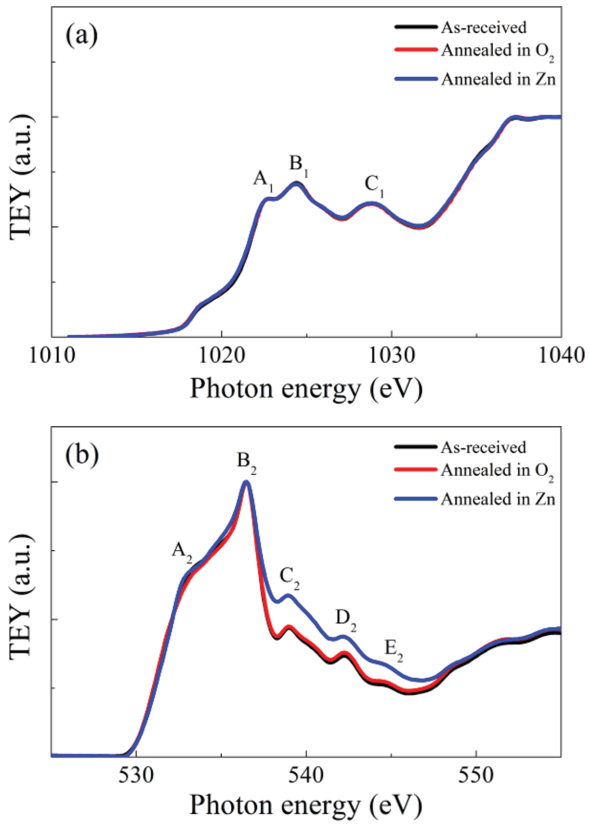

Figure 3. Normalized a) Zn L_3-edge and b) O *K*-edge XANES spectra of ZnO nanoparticles annealed at 900 °C under O_2 and Zn vapor. The spectra were collected in surface sensitive TEY mode. There are no additional Zn-related defects during annealing, however, V_O is formed in Zn vapor anneal.

Figure 3a. These spectra exhibit three peaks labeled A_1, B_1, and C_1 at 1022.7, 1024.3, and 1028.9 eV, respectively, which mainly reflect the electron transitions from Zn $2p_{3/2} \rightarrow 4s$, $5s$ and Zn $2p_{3/2} \rightarrow 3d$ derived states in the CB.[32] The Zn L_3-edge spectra are virtually identical in all three samples, indicating that the atomic configurations of Zn atoms are unaffected following the coalescence of nanoparticles. This result confirms that no additional Zn-related defects such as Zn interstitials are introduced during Zn vapor annealing presumably because of the high mobility of Zn_i.

Figure 3b shows the O K-edge XANES of the ZnO nanoparticles, which were normalized in the energy range of 550–555 eV. The spectra show five resolvable features labeled A_2, B_2, C_2, D_2, and E_2 at 533.5, 536.5, 539.0, 542.0, and 544.6 eV, respectively. The spectral features predominantly reflect the O $2p$ unoccupied states and their hybridization with Zn orbitals. Features A_2 and B_2 are mainly attributable to the hybridization of O $2p$ and highly dispersive Zn $4s$ in ZnO.[33] Features C_2, D_2, and E_2 are attributed to electron transitions from O $1s$ to unoccupied O $2p$, hybridized with Zn $4p$ and $4d$ states.[34,35] Upon annealing in Zn vapor, the intensities of C_2, D_2, and E_2 increase significantly. It has been recently established that stronger antibonding interactions of O $2p$ and Zn $4p$ states are formed due to a lattice distortion caused by V_O which affects its shell of surrounding O atoms.[36] Consequently, the increase in C_2, D_2, and E_2 features

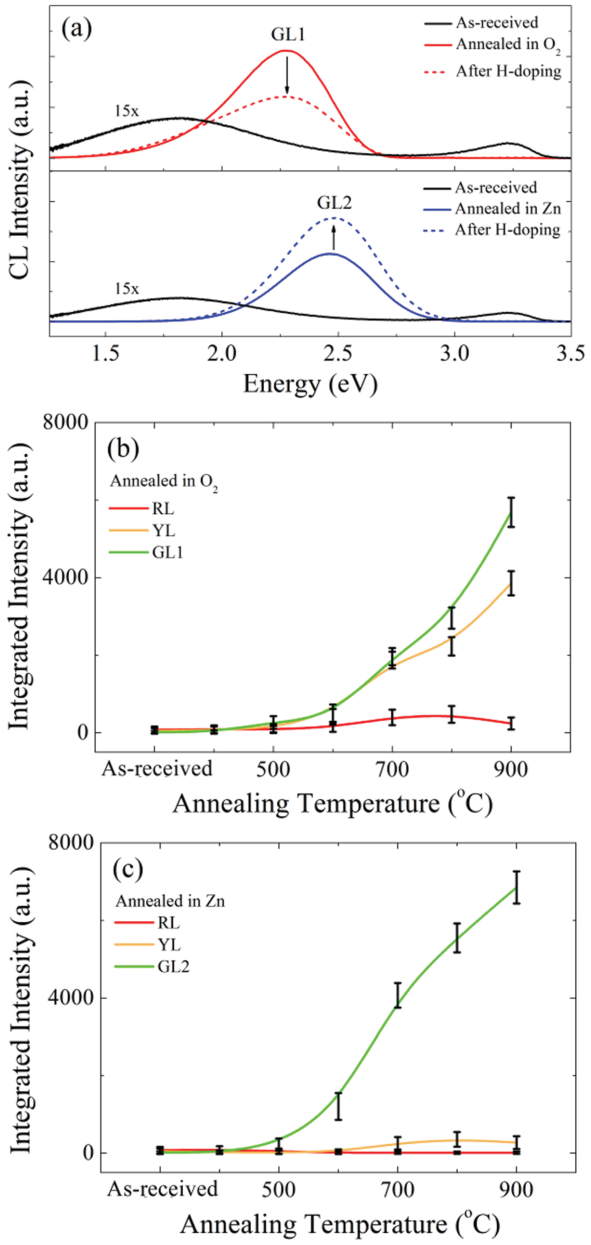

Figure 4. a) CL spectra of O_2 and Zn annealed nanoparticles, recorded at 80 K. The Zn vapor annealed GL2 at 2.28 eV increases following H^+ plasma treatment, whereas the O_2 annealed GL1 at 2.48 eV is quenched after the same treatment. Thermal evolution of RL, YL, GL1, and GL2 emissions as a function of annealing temperature in b) O_2 and c) Zn vapor atmosphere. GL1 and GL2 arises from thermally generated V_{Zn} and V_O related centers, respectively.

are attributed to the presence of a high concentration of surface oxygen vacancies, supporting the EPR $g = 2.00$ assignment to these centers. This interpretation is consistent with the work of Krishnamurthy et al.[37] Nanoparticles annealed in Zn vapor at 700 °C show similar behavior (See Figure S3, Supporting Information).

We now report the optical properties of the defects in the nanoparticles. **Figure 4**a shows the effects of annealing at 900 °C and hydrogen doping on the cathodoluminescence (CL)

properties of the ZnO nanoparticles. The deep-level CL emission of the as-received ZnO nanoparticles at 80 K exhibits a broad visible band centered at 1.82 eV. Annealing in O_2 atmosphere induces strong GL at 2.28 eV (GL1), while Zn vapor annealing produces a green peak centered at 2.48 eV (GL2). The emission intensity of these two GL bands change in an opposite manner in response to a mild H-plasma treatment: decreasing GL1 and increasing GL2, confirming these emissions are of different chemical origin. Quenching GL1 following incorporation of H^+ donors suggests that this emission is related to an acceptor-like defect. The V_{Zn}^{2-} defect is a likely candidate because, as a double acceptor, it will preferentially interact with H^+ donors forming $(H-V_{Zn}^{2-}-H)$ complexes.[38] Assignment of GL1 to V_{Zn}^{2-} is consistent with the absence of a corresponding EPR signal in Figure 2 as this defect has no unpaired electrons. Additionally XANES measurements show that the presence of V_{Zn}^{2-} does not strongly affect the atomic configuration of Zn in the ZnO nanoparticles. Zn vapor annealing leads to an increase in the concentration of V_O due to surface chemical reactions, as confirmed by the EPR and XANES results presented above, since the nanoparticles coalesce in a zinc rich environment.[39] GL2 can therefore logically be assigned to the formation of surface V_O centers, rather than changes in nanoparticle morphology. In a control study carried out in inert gas Ar at the same annealing temperatures, the nanoparticles exhibit similar faceted morphologies and coalescence behavior as in Zn vapor anneal (see Figures 1 and S2, Supporting Information), albeit at a slightly slower growth rate. The comparatively larger particle sizes when annealing in Zn vapor environment are due to the efficient diffusion of Zn_i in ZnO at elevated temperatures.[40] Enhancement of GL2 following exposure to H^+ can be explained by H passivation nonradiative recombination channels. This interpretation is supported by the increase of the intensity of the near band edge which doubled after H doping. Previous work by other authors showed that GL decreases with increasing particle size, due to holes trapped at the ZnO surface.[41,42] However, no such size dependence was observed in this work, presumably because the particle size range in our study is approximately two orders of magnitude greater than the nanoparticle size in the earlier work (≈1 nm). Moreover, the fact that the GL2 CL spectral shape remains unaltered with the increase in the size of annealed ZnO nanoparticles confirms that V_O surface defects are not influenced by particle size.

It is known that the broad optical emission from ZnO is a superposition of multiple deep-level bands involving native and extrinsic defects. Nonlinear least squares curve fitting was applied to extract intensities of individual emissions from the broad defect band. To overcome uncertainty in curve fitting, reference Li-doped ZnO was used to establish the peak parameters of the common yellow emission in ZnO at 80 K, which yields the peak position and FWHM of 1.96 and 0.56 eV, respectively.[43,44] These parameters were constrained during curve fitting to provide rigorous fitting solutions to the deep-level band (see Figure S4, Supporting Information). Using this constrained fitting approach, we were able to establish the intensities of red luminescence (RL), YL, and GL in the nanoparticles as a function of annealing temperature as shown in Figure 4b,c. GL1 and GL2 are dominant in O_2 and Zn vapor anneals, respectively. Furthermore, GL1 and GL2 defects can be

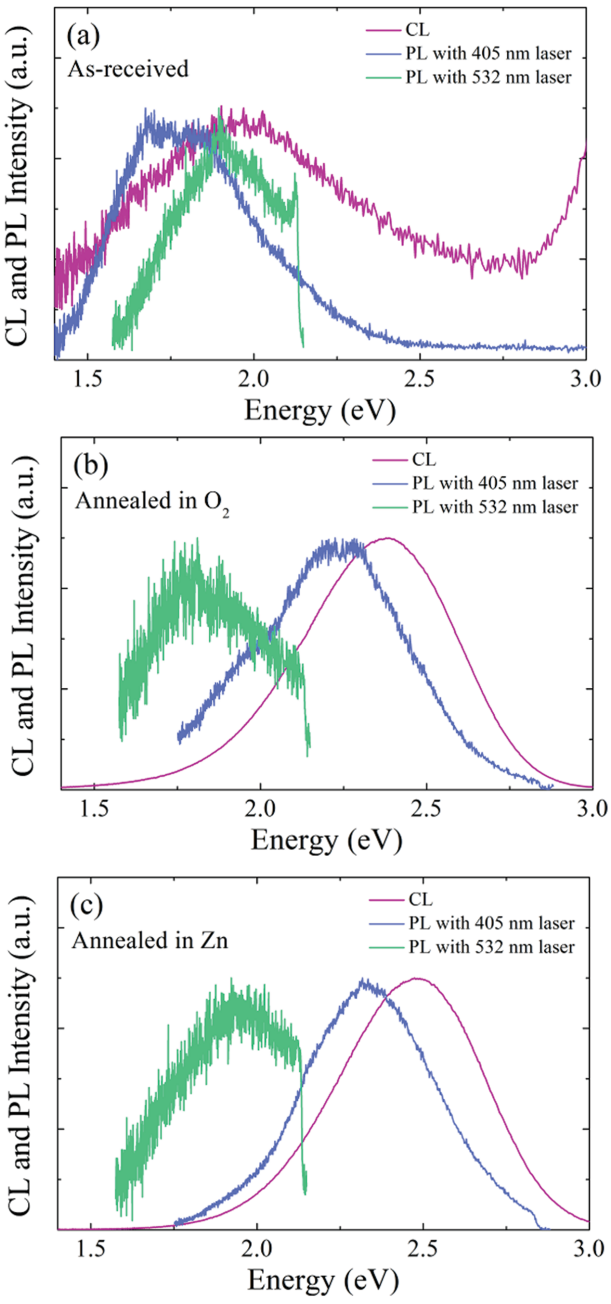

Figure 5. Comparison of steady-state 532 and 405 nm laser excitation PL and CL spectra at 300 K for a) as-received as well as b) and c) for ZnO nanoparticles annealed at 900 °C in O_2 and Zn vapor, respectively. The sharp feature is due to the presence of an edge filter.

engineered by employing two-stage annealing in two different gaseous environments, as illustrated in Figure S5, Supporting Information. When annealing at 900 °C, the V_{Zn}-related GL1 in O_2-annealed nanoparticles is completely quenched by Zn vapor and the spectrum becomes predominantly GL2, while the V_O-related GL2 of Zn-annealed nanoparticles is gradually reduced and shifted towards GL1. The rapid annihilation of V_{Zn} defects upon annealing in Zn vapor can be attributed to the high mobility of Zn_i at temperatures above 400 °C.[26] These results

Adv. Optical Mater. 2015,
DOI: 10.1002/adom.201400592

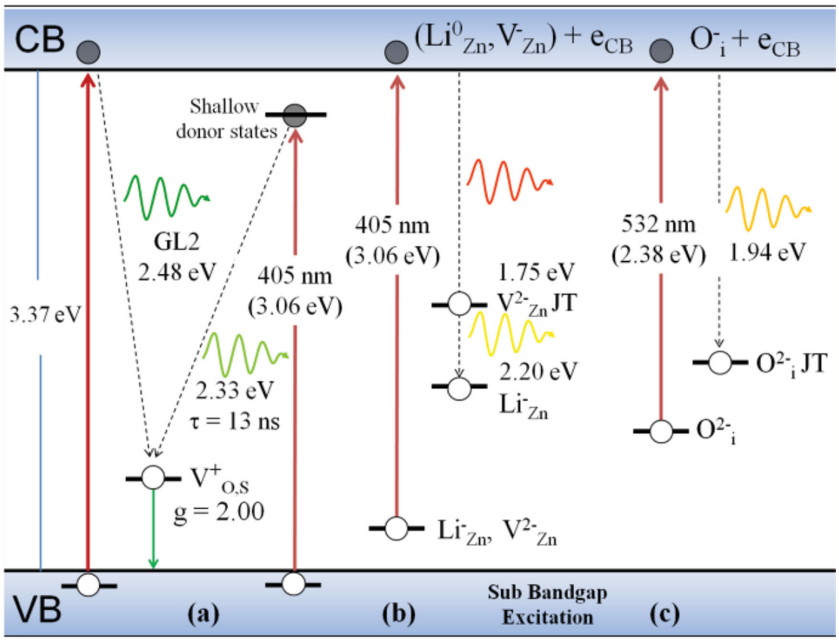

Figure 6. Band diagram showing the possible excitation and emission pathways from the discussed defect states. Dashed lines indicate radiative pathways while solid red lines indicate excitation. a) GL2 emission at 2.48 eV produced with above (CL) and 2.33 eV emission generated with sub-bandgap 405 nm excitation laser, where valence band electrons are promoted to the CB and shallow donor states, respectively, b) promotion of electrons from ionized Li_{Zn}^{-} and V_{Zn}^{2-} acceptors to the CB (photoionization) using sub-bandgap 405 nm light forming Li_{Zn}^{0} and V_{Zn}^{-} and a CB electron (e_{CB}) and the ensuing radiative recombination reinstating the Li_{Zn}^{-} and V_{Zn}^{2-} with PL at 2.23 and 1.75 eV, respectively. The later has a large Stokes shift due to a JT distortion[45] and c) photoionization and radiative relaxation of ionized oxygen interstitials, O_i^{2-} using sub-bandgap 532 nm light to produce PL at 1.94 eV.

indicate that V_{Zn} and V_O can be eliminated by reductive and oxidative anneal, respectively.

Figure 4b shows a significant difference in the thermal behavior of Li-related YL, which increases drastically in O_2 anneal while the RL is only slightly affected. The rise in the YL in O_2 anneal is due to an increase in the number of Li_{Zn} acceptors that can be explained by V_{Zn} defects being occupied by mobile Li_i with increasing temperature via the following defect reaction, $Li_i + V_{Zn} \rightarrow Li_{Zn}$. Conversely annealing in Zn vapor produces a strong enhancement of GL2 but only a modest rise in YL and no change in the RL (Figure 4c). This behavior is different to O_2 anneal due to the growth of the nanoparticles in Zn vapor (oxygen deficient) atmosphere. These results further confirm that GL1 and GL2 have a different chemical origin: GL2 results from recombination channels involving V_O defects while GL1 is related to V_{Zn} centers. The formation of point defects upon annealing at high temperatures (> 500 °C) can be described as the following:

$$Zn(g) \rightarrow Zn_{Zn} + V_{O,s} \text{(reductive anneal in Zn vapor)}$$

$$\frac{1}{2}O_2(g) \rightarrow O_O + V_{Zn} \text{(oxidative anneal in } O_2\text{)}$$

It is noteworthy that after one year of storage the samples in air the CL spectra of the annealed ZnO nanoparticles are unchanged, indicating that the point defects are stable in air.

Finally we discuss the photophysics of the defect-related luminescence emissions. Here, we perform photoluminescence (PL) measurements using sub-bandgap 405 and 532 nm laser excitation to directly access the deep level defects in the ZnO nanoparticles. Normalized sub-bandgap PL spectra and above bandgap CL spectra at 300 K for the as-received, Zn and O_2 annealed samples are shown in **Figure 5**. When excited using the 405 nm laser PL peaks are observed at 2.33 eV (Zn vapor anneal), 2.23 eV (O_2 anneal), and 1.75 eV (as-received). The last two peaks can be attributed to photoionization and radiative relaxation transitions involving ionized Li_{Zn}^{-} and V_{Zn}^{2-} acceptors, respectively.[45,46] The large Stokes shift with the 1.75 eV as been explained by strong Jahn–Teller (JT) distortion of the V_{Zn}^{-} center.[45] The first peak at 2.33 eV has not been reported in the literature, consequently it is assigned to a radiative transition between photoexcitation of carriers in donor states below the CB with deeply trapped holes at surface oxygen vacancies. Sub-bandgap excitation with the 532 nm laser at 300 K on the other hand produces a PL peak around 1.90 eV in all three samples, which has been ascribed to oxygen interstitials, O_i.[46] The excitation and radiative decay of all of sub-bandgap and above bandgap electronic transitions for each of the defects described above are illustrated in **Figure 6**. The fact that the same defects (i.e., V_{Zn} and V_O) can be accessed using either sub-bandgap excitation or above bandgap excitation, exemplifies that these defects provide very efficient radiative recombination pathways. This is important for future integration of these defects with electrically stimulated devices and photonic resonators.[47]

Figure 7a shows the excited state lifetimes of the fluorescent defects excited by sub-bandgap 405 nm excitation. The as-received nanoparticles and Zn annealed nanoparticles exhibit a similar short lifetime of $\tau = 10 \pm 0.3$ ns and $\tau = 13 \pm 0.4$ ns for the 1.75 and 2.32 eV emission respectively. The sub-bandgap emission at 2.22 eV formed under O_2 annealing displayed a much longer decay time of $\tau > 1$ µs, confirming that the 2.23 eV peak has a different chemical origin to the PL peaks at 2.33 and 1.75 eV. The very slow decay time and position of this emission is consistent with reported optical properties for the Li_{Zn} center[48] observed in the CL data Figure 4b. PL decay curves of the ≈1.90 eV center excited by 514 nm laser light are shown in Figure 7b exhibiting short lifetimes of $\tau = 3.55 \pm 0.17$ ns, $\tau = 3.60 \pm 0.12$ ns, and $\tau = 3.50 \pm 0.16$ ns for the as-received, O_2 and Zn vapor annealed samples, respectively. These sub-bandgap excitation data indicate that the relaxation of the excited states occurs through very fast nonradiative channels, which enable the system to be efficiently reexcited. This can occur through fast internal phononic relaxation. A complete understanding of the sub-bandgap

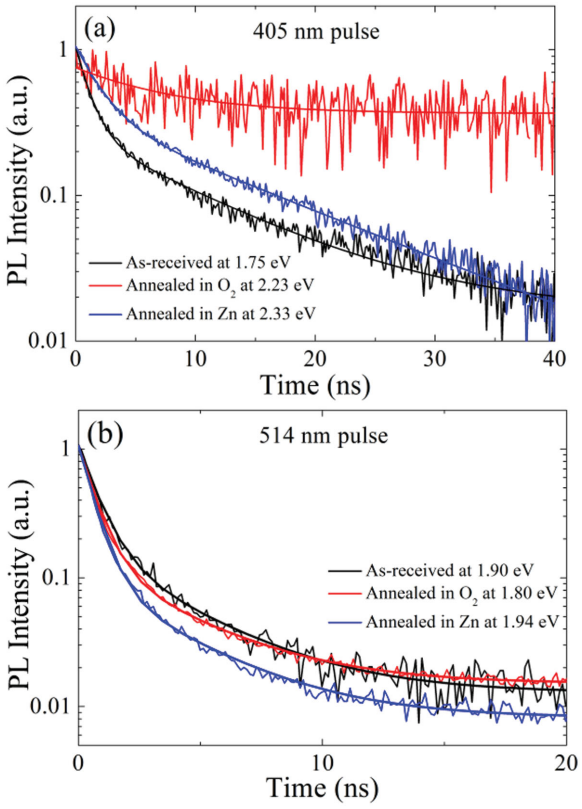

Figure 7. PL decay curves at 300 K acquired with a) 405 nm and b) 514 nm laser pulse for corresponding nanoparticles shown in Figure 5.

excitation and emission PL transitions would require detailed resonant studies of single V_{Zn} and V_O.

3. Conclusion

In summary, we have undertaken detailed correlative CL, PL, EPR, and XANES studies of radiative defects in ZnO nanoparticles. An optical emission peak at 2.28 eV has been attributed to a V_{Zn} related center while an emission at 2.48 eV and corresponding EPR signal at $g = 2.00$ has been assigned to surface V_O^+ centers. Their properties at 300 K are summarized in **Table 1**. These radiative point defects can be excited using both above bandgap and sub-bandgap excitation which is beneficial for devices and different centers exhibit lifetimes ranging from nanoseconds to microseconds. These exciting luminescence properties of ZnO nanostructures are important to the future development of ZnO materials for nanophotonics, optoelectronics, and quantum applications.

4. Experimental Section

To generate the defects within the ZnO nanoparticles (Nanostructured and Amorphous Materials Inc., USA), several annealing treatments were applied. ZnO nanoparticles were first annealed for 1 h at temperatures between 400 and 900 °C in pure O_2 and Zn vapor with a flow rate of 20 sccm at a pressure of 1 atm. The Zn vapor ambient was generated using a metallic Zn source held just above its melting point (420 °C) upstream from the ZnO nanoparticles with argon as the carrier gas. To probe the charge state of defects, the nanoparticles were doped with hydrogen by exposure to a mild hydrogen radio-frequency plasma (15 W, sample temperature 473 K) for 3 min. Hydrogen is known to exist exclusively as a positively charged donor in ZnO[49] and expected to interact strongly with negatively charged defects.

The EPR measurements were made using a Bruker Elexys E500 cw X-band EPR spectrometer equipped with an Oxford ITC605 temperature controller. All presented EPR spectra were collected at 10 K using a power of 2.0 mW with a modulation amplitude of 5.0 G and a frequency of 9.4 GHz. The local surface electronic structure around Zn and O atoms in ZnO nanoparticles before and after annealing process was studied using an X-ray absorption near edge structure (XANES) technique. XANES implemented in the Total Electron Yield (TEY) mode was performed around the Zn L_3-edge and O K-edge on the Soft X-ray Spectroscopy beamline, Australian Synchrotron. The photon energy scale was calibrated against the Au $4f_{7/2}$ peak at 84 eV from a clean gold film in electrical contact with samples.

The samples were characterized by CL spectroscopy at 80 K using a FEI Quanta 200 Environmental SEM equipped with a liquid nitrogen cold stage and an Ocean Optics SD2000 Diode Array Optical Spectrometer. For CL measurements, the accelerating voltage was fixed at 15 kV and the electron beam current was 0.25 nA. All spectra were corrected for the total response of the light collection and measurement system. The PL spectra of the annealed ZnO nanoparticles were collected using a home built confocal microscope with 500 nm resolution. The excitation was performed using a continuous wave laser ($\lambda = 405$ nm) through a high numerical aperture (NA = 0.9) objective. The signal was collected using the same objective and directed into a spectrometer (Princeton Instruments, 300 lines/nm grating). For the time-resolved measurements, a picoseconds pulsed laser ($\lambda = 405$ nm, repetition 20 MHz) was employed. The signal was recorded using an Avalanche Photo Diode (Excelitas, SPCM-AQRH-14) and analyzed using a time-Correlated Single Photon Counting (PicoHarp 300) with 64 ps resolution. In all cases, a dichoric mirror was used to filter the excitation laser, and a band pass filter to select only the defect emission. The measurements were done at room temperature.

Supporting Information

Supporting Information is available from the Wiley Online Library or from the author.

Table 1. Summary of luminescent point defects in ZnO nanoparticles and their photophysical properties.

Sample	Emission energy [eV] and lifetime at 300 K			EPR	H-plasma effect on CL
	Above bandgap CL	Sub-bandgap PL 405 nm	Subbandgap PL 532 nm	g-factor	
Zn vapor anneal GL2	2.48 Surface V_o^+	2.33 shallow donors – surface V_o^+, $\tau = 13$ ns	1.94 O_i, $\tau = 3.6$ ns	2.00	Quenched
Oxygen anneal GL1	2.38 V_{Zn} center	2.2 Li_{Zn}, $\tau = > 1$ µs	1.80 O_i, $\tau = 3.6$ ns	None	Enhanced
As-received	1.96 O_i	1. 75 shallow donors – V_{Zn} related center, $\tau = 10$ ns	1.90 O_i, $\tau = 3.5$ ns	None	Quenched

Adv. Optical Mater. **2015**,
DOI: 10.1002/adom.201400592

Acknowledgements

This research was undertaken on the Soft X-ray Spectroscopy beamline at the Australian Synchrotron, Australia. We acknowledge the technical assistance of L. Thomsen and A. Tadich at the Australian Synchrotron. I.A. is the recipient of an Australian Research Council Discovery Early Career Research Award (Project No. DE130100592). S.P. thanks Prof. Marina Bennati at Max-Planck Institute for Biophysical Chemistry for access to the EPR facility.

Received: December 10, 2014
Revised: January 14, 2015
Published online:

[1] M. H. Huang, S. Mao, H. Feick, H. Yan, Y. Wu, H. Kind, E. Weber, R. Russo, P. Yang, *Science* **2001**, *292*, 1897.
[2] R. Könenkamp, R. C. Word, C. Schlegel, *Appl. Phys. Lett.* **2004**, *85*, 6004.
[3] Ü. Özgür, Y. I. Alivov, C. Liu, A. Teke, M. Reshchikov, S. Doğan, V. Avrutin, S.-J. Cho, H. Morkoc, *J. Appl. Phys.* **2005**, *98*, 041301.
[4] C. Rauch, W. Gehlhoff, M. Wagner, E. Malguth, G. Callsen, R. Kirste, B. Salameh, A. Hoffmann, S. Polarz, Y. Aksu, *J. Appl. Phys.* **2010**, *107*, 024311.
[5] R. Cox, D. Block, A. Hervé, R. Picard, C. Santier, R. Helbig, *Solid State Commun.* **1978**, *25*, 77.
[6] K. Vanheusden, C. Seager, W. t. Warren, D. Tallant, J. Voigt, *Appl. Phys. Lett.* **1996**, *68*, 403.
[7] A. Kohan, G. Ceder, D. Morgan, C. G. Van de Walle, *Phys. Rev. B* **2000**, *61*, 15019.
[8] M. Liu, A. Kitai, P. Mascher, *J. Lumin.* **1992**, *54*, 35.
[9] D. C. Reynolds, D. C. Look, B. Jogai, H. Morkoc, *Solid State Commun.* **1997**, *101*, 643.
[10] N. Garces, L. Wang, L. Bai, N. Giles, L. Halliburton, G. Cantwell, *Appl. Phys. Lett.* **2002**, *81*, 622.
[11] S. Choi, B. C. Johnson, S. Castelletto, C. Ton-That, M. R. Phillips, I. Aharonovich, *Appl. Phys. Lett.* **2014**, *104*, 261101.
[12] A. J. Morfa, B. C. Gibson, M. Karg, T. J. Karle, A. D. Greentree, P. Mulvaney, S. Tomljenovic-Hanic, *Nano Lett.* **2012**, *12*, 949.
[13] N. Jungwirth, Y. Pai, H. Chang, E. MacQuarrie, G. Fuchs, *J. Appl. Phys.* **2014**, *116*, 043509.
[14] H. Yang, S. Lau, S. Yu, A. Abiyasa, M. Tanemura, T. Okita, H. Hatano, *Appl. Phys. Lett.* **2006**, *89*, 011103.
[15] Q. Wan, Q. Li, Y. Chen, T.-H. Wang, X. He, J. Li, C. Lin, *Appl. Phys. Lett.* **2004**, *84*, 3654.
[16] J. L. O'Brien, A. Furusawa, J. Vučković, *Nat. Photonics* **2009**, *3*, 687.
[17] S. Polarz, A. Roy, M. Merz, S. Halm, D. Schröder, L. Schneider, G. Bacher, F. E. Kruis, M. Driess, *Small* **2005**, *1*, 540.
[18] R. K. Sendi, S. Mahmud, *Appl. Surf. Sci.* **2012**, *261*, 128.
[19] Y. Gu, I. L. Kuskovsky, M. Yin, S. Obrien, G. Neumark, *Appl. Phys. Lett.* **2004**, *85*, 3833.
[20] A. Pöppl, G. Völkel, *Phys. Status Solidi A* **1991**, *125*, 571.
[21] A. B. Djuriši , Y. H. Leung, W. C. Choy, K. W. Cheah, W. K. Chan, *Appl. Phys. Lett.* **2004**, *84*, 2635.
[22] C. Geisler, G. Simmons, *Phys. Lett.* **1964**, *11*, 111.
[23] G. Neumann, in *Current Topics in Materials Science* (Ed.: E. Kaldis), North-Holland, Amsterdam **1981**, p. 269.
[24] L. Larina, N. Tsvetkov, J. Yang, K.-S. Lim, O. Shevaleevskiy, *ECS Trans.* **2010**, *28*, 161.
[25] J. Smith, W. Vehse, *Phys. Lett.* **1970**, *31A*, 147.
[26] A. Janotti, C. G. Van de Walle, *Phys. Rev. B* **2007**, *76*, 165202.
[27] G. Neumann, in *Current Topics in Materials Science* (Ed.: E. Kaldis), North-Holland, Amsterdam **1981**, p. 279
[28] P. Erhart, K. Albe, *Appl. Phys. Lett.* **2006**, *88*, 201918.
[29] D. Galland, A. Herve, *Phys. Lett.* **1970**, *33A*, 1.
[30] L. Hu, J. Huang, H. He, L. Zhu, S. Liu, Y. Jin, L. Sun, Z. Ye, *Nanoscale* **2013**, *5*, 3918.
[31] D. M. Murphy, in *Metal Oxide Catalysis* (Eds: S. D. Jackson, J. S. J. Hargreaves), Wiley VCH Verlag GmbH & Co. KGaA, Weinheim, Germany **2008**, p. 150.
[32] J. Chiou, J. Jan, H. Tsai, C. Bao, W.-F. Pong, M.-H. Tsai, I.-H. Hong, R. Klauser, J. Lee, J. Wu, *Appl. Phys. Lett.* **2004**, *84*, 3462.
[33] A. P. Singh, R. Kumar, P. Thakur, N. Brookes, K. Chae, W. Choi, *J. Phys: Condens. Matter* **2009**, *21*, 185005.
[34] J. Chiou, K. Kumar, J. Jan, H. Tsai, C. Bao, W.-F. Pong, F. Chien, M.-H. Tsai, I.-H. Hong, R. Klauser, *Appl. Phys. Lett.* **2004**, *85*, 3220.
[35] C. Dong, C. Persson, L. Vayssieres, A. Augustsson, T. Schmitt, M. Mattesini, R. Ahuja, C. Chang, J.-H. Guo, *Phys. Rev. B* **2004**, *70*, 195325.
[36] Y. Kim, S. Kang, *Acta Mater.* **2011**, *59*, 126.
[37] S. Krishnamurthy, C. McGuinness, L. Dorneles, M. Venkatesan, J. Coey, J. Lunney, C. Patterson, K. Smith, T. Learmonth, P.-A. Glans, *J. Appl. Phys.* **2006**, *99*, 08M111.
[38] E. Lavrov, J. Weber, F. Börrnert, C. G. Van de Walle, R. Helbig, *Phys. Rev. B* **2002**, *66*, 165205.
[39] G. Xing, X. Fang, Z. Zhang, D. Wang, X. Huang, J. Guo, L. Liao, Z. Zheng, H. Xu, T. Yu, *Nanotechnology* **2010**, *21*, 255701.
[40] P. Erhart, K. Albe, *Appl. Phys. Lett.* **2006**, *88*, 201918.
[41] L. Zhang, L. Yin, C. Wang, N. Lun, Y. Qi, D. Xiang, *J. Phys. Chem. C* **2010**, *114*, 9651.
[42] A. Van Dijken, J. Makkinje, A. Meijerink, *J. Lumin.* **2001**, *92*, 323.
[43] L. L. Lem, M. R. Phillips, C. Ton-That, *J. Lumin.* **2014**, *154*, 387.
[44] M. R. Phillips, K. E. McBean, G. McCredie, C. Ton-That, at the European Materials Research Society, Warsaw, Poland **2009**.
[45] X. Wang, L. Vlasenko, S. Pearton, W. Chen, I. A. Buyanova, *J. Phys. D: Appl. Phys.* **2009**, *42*, 175411.
[46] M. Willander, O. Nur, J. R. Sadaf, M. I. Qadir, S. Zaman, A. Zainelabdin, N. Bano, I. Hussain, *Materials* **2010**, *3*, 2643.
[47] G. Shambat, B. Ellis, A. Majumdar, J. Petykiewicz, M. A. Mayer, T. Sarmiento, J. Harris, E. E. Haller, J. Vučković, *Nat. Commun.* **2011**, *2*, 539.
[48] M. Reshchikov, H. Morkoc, B. Nemeth, J. Nause, J. Xie, B. Hertog, A. Osinsky, *Physica B* **2007**, *401*, 358.
[49] C. G. Van de Walle, J. Neugebauer, *Nature (London)* **2003**, *423*, 626.